The 9th European Congress on Computational Methods in Applied Sciences and Engineering
ECCOMAS Congress 2024
3–7 June 2024, Lisboa, Portugal

DETERMINATION OF NEUTRAL AXIS AND EFFECT OF VARIATION OF CROSS SECTIONAL AREA ON THE MECHANICAL PROPERTIES OF SMART META-STRUCTURE

SUBHADEEP SAHANA[1,a], **AMANPREET SINGH**[1,b] **AND BISHAKH BHATTACHARYA**[1,c]

[1] Department of Mechanical Engineering, Indian Institute of Technology Kanpur, India

[a] subhadeeps21@iitk.ac.in, [b] amangill@iitk.ac.in, [c] bishakh@iitk.ac.in

Key words: Active honeycomb lattices, Magnetostrictive material, Smart material, Elastic properties of lattices, Structural properties

Summary. In recent years, manufacturing has paved the way to enhance structural properties using 3D printed structures by constructing complex shapes. The properties of such structures depend on the arrangement of the internal lattices. Honeycomb is one such simple lattice structure that is widely used by researchers as it exhibits a high strength-to-weight ratio. However, the elastic properties of the lattice structures are intrinsic functions of the material properties and the geometric shape. Hence, it is impossible to modulate the elastic properties once constructed. Recent studies have shown that the active modulation of the elastic properties can be achieved by incorporating smart materials over the substrate layers of the lattice. The analytical expressions have been developed for honeycomb/ auxetic honeycomb lattice considering the Euler-Bernoulli bi-layer beam to determine its elastic properties. The expression is well valid for lattices where the thickness of the smart material is relatively less compared to the substrate thickness. However, it does not produce consistent results as the thickness of the smart material increases due to the shift of the position of the neutral axis, which was earlier assumed to be at the geometric centre of the substrate beam. This paper presents a modified formulation that considers the change in the position of the neutral axis as the thickness of the smart material patches varies. This modification allows the use of the analytical expression for beams with higher thickness ratios and can be used to understand the impact of forces in shear deformation. In addition, the variation in the elastic properties has also been investigated for different cross-sectional shapes such as I-section, T-section, and rectangular cross-section. The formulation presented here is generic, and the concept can be used in various futuristic multi-functional structural systems and devices across different length scales.

1 INTRODUCTION

Latticed materials have gained significant interest among researchers in the past few years. Various 1D/2D/3D shapes are repeated periodically to develop such structures. Unlike conventional material, where the composition of the material is solely responsible for the overall properties,

in latticed metamaterial, the pattern of the unit cell also influences the same. The unique pattern of the structure leads to the development of some properties that may not be observed with conventional material. This group of materials is popularly known as metamaterial. Such materials can exhibit properties like auxeticity [1], which refers to the unusual behaviour of expanding along perpendicular directions when stretched rather than contracting like most materials. It can manipulate band gap characteristics [2, 3], allowing transmission of certain frequencies of electromagnetic waves. The structure can serve as an effective wave guide [4], confining and directing the propagation of waves along specific paths. Mechanical metamaterials are subset of this domain that deals with the mechanical characteristics of the structure. These materials exhibit interesting properties like zero or negative Poisson's ratio [5], negative compressibility [6], and vanishing shear modulus [7], which are all exceptions from the common behaviour of natural materials. Honeycomb is preferred over other structures due to its high strength-to-weight ratio [8].

Recent studies have shown that it is possible to change the structural properties by varying the unit cell features. Gibson et.al. [9] did a generic study on the properties of honeycomb and the dependence on its structural parameters. Closed-form expressions of mechanical properties like Young's modulus and Poisson's ratio were formulated. Several authors tried to alter the geometric features passively to modulate the properties. Hierarchical structures were used to modulate the characteristics by adjusting dimension ratios of different hierarchy [10]. A programmable deformation-dependent stiffness and shape modulation using distant actuation can be generated using an origami structure [11]. Recent literature also revealed the existence of negative Young's modulus and Poisson's ratio in some structures [12, 13].

However, active modulation of the properties can better impact the development of futuristic materials as the structure reacts to an unknown externally applied stimulus. Magnetic insertion can be used within the structure for tuning the geometry and to ultimately have active control over the macroscopic property of the structure [14]. Moreover, smart materials like piezoelectric material, which changes dimensions in electric fields, can be integrated with the substrate material [15]. A voltage-dependent metamaterial with a close form expression of the apparent elastic property was thus developed [16]. Similarly, contactless metamaterial was developed using magnetostrictive material over the substrate material [17], which provides active control of structural properties in a contactless fashion. The magnetostrictive material referred to here changes its dimension in the presence of the magnetic field. However, the current modelling of smart material-based structures [16, 17] have limitations with the thickness of the smart layer. The results become inconsistent as the thickness increased beyond some thickness ratio depending upon the smart material used. This limitation has been corrected in our research paper, wherein a new model has been proposed that gives a consistent result, thus generalizing the expression. Further, a study was conducted on the change in the cross-sectional shapes of the lattice structure, and property variation was observed.

The remainder of the paper is organized as follows: section 2 provides a concise overview and presents the derivation of the generalized structure. Various cross-sectional shapes are considered in Section 3, and the structures were analyzed to develop closed-form expression of apparent elastic properties. In Section 4, the focus is on the comparison of the new model with the existing literature and the variation in the elastic properties as the cross-sectional shape varies.

Finally, concluding remarks are summarized in Section 5.

2 DERIVATION

A bottom-up approach is used to derive the apparent structural properties. The lattice used here is a periodic arrangement of a unit cell. Thus, a unit cell is formulated, expanding the idea to the whole structure. The unit cell comprises the substrate material layered by a smart material in an unimorph condition, as represented in Fig. 1. The unit cells are assumed to be made up of Euler-Bernoulli beams, and the displacement in the $x-z$ plane can be represented as

$$u(x,z,t) = u^0(x,t) - zw^0_{,x}(x,t) \tag{1}$$

$$w(x,t) = w^0(x,t) \tag{2}$$

Strain equation can be written using Eqn. 1 and Eqn. 2 as

$$\begin{aligned} \varepsilon_x &= \frac{\partial u^0(x,t)}{\partial x} - z\frac{\partial^2 w^0(x,t)}{\partial x^2} \\ \varepsilon_y, \varepsilon_z, \varepsilon_{xy}, \varepsilon_{yz}, \varepsilon_{xz} &= 0 \end{aligned} \tag{3}$$

Stress in the substrate beam is

$$\sigma_s = Y_s \varepsilon_x \tag{4}$$

Stress in magnetostrictive patch is given as

$$\sigma_m = Y_m (\varepsilon_x - dH) \tag{5}$$

where, Y_s is Young's modulus of the substrate, Y_m is Young's modulus of the magnetostrictive material, d is the magnetostrictive constant and H is the applied magnetic field intensity.
Potential energy in the unit cell is thus given as

$$U_c = \frac{1}{2}\left(\int_{V_s} \sigma_x \varepsilon_x dV_s + \int_{V_m} \sigma_m \varepsilon_x dV_m\right) \tag{6}$$

Magnetic energy in the unit cell is given as

$$U_m = \frac{W_s}{2}\left(\int_0^L \int_{\frac{T_s}{2}}^{T_m} \mu H^2 dz dx\right) \tag{7}$$

where, W_s is the width of substrate, T_s is thickness of substrate, T_m is thickness of smart layer and μ is the magnetic permeability.
Hamilton's principle is applied to Eqn. 6 and Eqn. 7 to derive the displacement equation for the two-node and three-DOF hybrid beam in the presence of the magnetic field. This is represented in matrix form as

$$\{q\}_{6\times 1} = [K]^{-1}_{6\times 6}\{F\}_{6\times 1} \tag{8}$$

With the consideration of one end of the beam fixed, appropriate boundary conditions are applied, and the force matrix (F) and stiffness matrix (K) of the hybrid beam [17] are given as

$$[F] = \begin{bmatrix} -F_m \\ 0 \\ M_m \\ F_m \\ 0 \\ -M_m \end{bmatrix}; \qquad [K] = \begin{bmatrix} A & 0 & -B & -A & 0 & B \\ 0 & 12C & 6CL & 0 & -12C & 6CL \\ -B & 6CL & 4CL^2 & B & -6CL & 2CL^2 \\ -A & 0 & B & A & 0 & -B \\ 0 & -12C & -6CL & 0 & 12C & -6CL \\ B & 6CL & 2CL^2 & -B & -6CL & 4CL^2 \end{bmatrix} \tag{9}$$

The expression of the force vector elements F_m and M_m are given as

$$F_m = \frac{Y_m A_m dH}{2}; \quad M_m = \frac{Y_m H_m dH}{2}; \tag{10}$$

and expression of A, B, C are given as

$$A = \frac{Y_s A_s + Y_m A_m}{L}, \quad B = \frac{Y_s H_s + Y_m H_m}{L}, \quad C = \frac{Y_s I_s + Y_m I_m}{L^3} \tag{11}$$

where, A is the cross-section area, H is first moment of area, I is second moment of area and the subscripts s is substrate, m is the magnetostrictive material.
The beam cross-section is assumed to be rectangular. The subsequent discussion considers various parameters as follows:

$$k_t = \frac{Y_m}{Y_s}; \quad \alpha_R = \frac{T_m}{T_{Rs}}; \quad \beta = \frac{h}{L}; \quad \gamma_R = \frac{T_{Rs}}{L}; \quad H_{rat} = \frac{H}{\sigma_1} \tag{12}$$

An extensional force P is applied on the ends of the unit cell along direction 1, as in Fig. 1a. The force is given as

$$P = \sigma_1 L(\beta + \sin\theta) W_{Rs} \tag{13}$$

The constants used in the stiffness matrix are now determined with the neutral axis positioned at the region of the cross-section with zero bending stress. Dimensions h_{R1}, h_{R2}, h_{R3} of Fig. 2a are first calculated as follows:

$$\begin{aligned} \int_s y dA = \overline{y_s} A_s = \left(\frac{T_{Rs}}{2} - h_1\right)(T_{Rs} W_{Rs}) \\ \int_m y dA = \overline{y_m} A_m = \left(T_{Rs} + \frac{T_m}{2} - h_1\right)(T_m W_{Rs}) \end{aligned} \tag{14}$$

$$Y_s \int_s y dA + Y_m \int_m y dA = 0 \tag{15}$$

Solving Eqn. 15 using Eqn. 14,

$$h_{R1} = \frac{T_{Rs}^2 + k_t T_m (2T_{Rs} + T_m)}{2(T_{Rs} + k_t T_m)}; \quad h_{R2} = \frac{T_{Rs}^2 + 2T_{Rs}T_m + k_t T_m^2}{2(T_{Rs} + k_t T_m)}; \quad h_{R3} = \frac{T_{Rs}^2 - k_t T_m^2}{2(T_{Rs} + k_t T_m)} \tag{16}$$

Based on this calculation, the cross-section area and first and second moment of area are calculated, and subsequently apparent Young's modulus of the structure is determined.

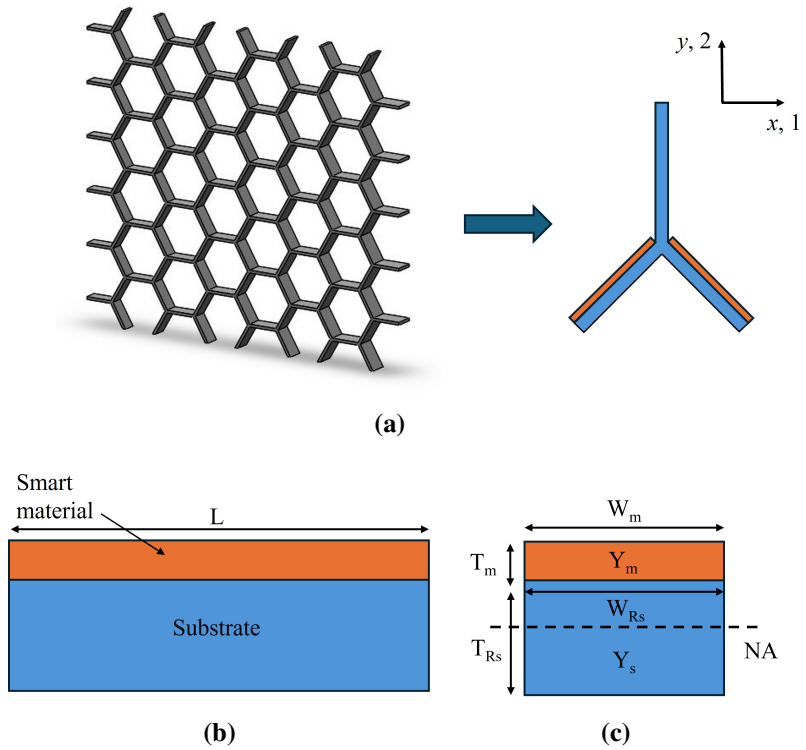

Figure 1: Unimorph configuration with rectangular cross-section **(a)** Honeycomb pattern and its unit cell **(b)** Front view **(c)** Cross section of each beam

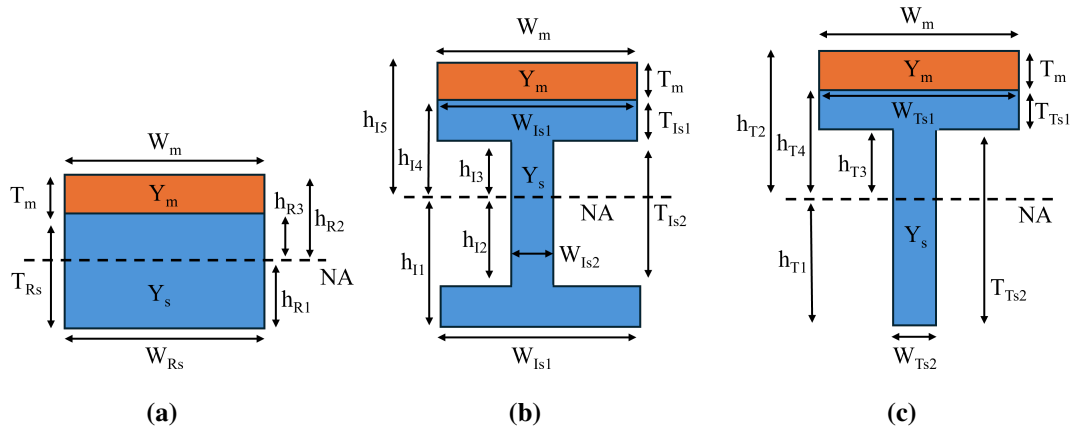

Figure 2: Various cross section of the composite structure **(a)** rectangular section **(b)** I-section **(c)** T-section

2.1 Substrate beam and smart layer parameters

In this section, we provide the closed form expressions of the Area, First and Second Moment of Inertia related to the passive beam and smart layer respectively. Accordingly, we obtained: Area of the beam

$$A_s = \int_0^{W_{Rs}} \int_{-h_{R1}}^{h_{R3}} dydx = W_{Rs}\left(\frac{-T_m^2 k_t + T_{Rs}^2}{2T_m k_t + 2T_{Rs}} + \frac{T_{Rs}^2 + k_t T_m(2T_{Rs} + T_m)}{2T_m k_t + 2T_{Rs}}\right)$$

First moment of inertia of beam

$$H_s = \int_0^{W_{Rs}} \int_{-h_{R1}}^{h_{R3}} zdydx = W_{Rs}\left(\frac{\left(-T_m^2 k_t + T_{Rs}^2\right)^2}{2(2T_m k_t + 2T_{Rs})^2} - \frac{\left(T_{Rs}^2 + k_t T_m(2T_{Rs} + T_m)\right)^2}{2(2T_m k_t + 2T_{Rs})^2}\right)$$

Second moment of inertia of beam

$$I_s = \int_0^{W_{Rs}} \int_{-h_{R1}}^{h_{R3}} z^2 dydx = W_{Rs}\left(\frac{\left(-T_m^2 k_t + T_{Rs}^2\right)^3}{3(2T_m k_t + 2T_{Rs})^3} + \frac{\left(T_{Rs}^2 + k_t T_m(2T_{Rs} + T_m)\right)^3}{3(2T_m k_t + 2T_{Rs})^3}\right)$$

Area of the smart layer

$$A_m = \int_0^{W_{Rs}} \int_{h_{R3}}^{h_{R2}} dydx = W_{Rs}\left(\frac{T_m^2 k_t + 2T_m T_{Rs} + T_{Rs}^2}{2T_m k_t + 2T_{Rs}} - \frac{-T_m^2 k_t + T_{Rs}^2}{2T_m k_t + 2T_{Rs}}\right)$$

First moment of inertia of smart layer

$$H_s = \int_0^{W_{Rs}} \int_{h_{R3}}^{h_{R2}} zdydx = \frac{W_{Rs} T_m T_{Rs}(T_m + T_{Rs})}{2T_m k_t + 2T_{Rs}}$$

Second moment of inertia of smart layer

$$I_s = \int_0^{W_{Rs}} \int_{h_{R3}}^{h_{R2}} z^2 dydx = \frac{W_{Rs} T_m \left(T_m^4 k_t^2 + 2T_m^3 T_{Rs} k_t + 4T_m^2 T_{Rs}^2 + 6T_m T_{Rs}^3 + 3T_{Rs}^4\right)}{12(T_m k_t + T_{Rs})^2}$$

Based on these geometric properties, in the following section, we obtained the apparent elastic properties of the latticed structure.

2.2 Calculation of apparent elastic properties

2.2.1 Longitudinal Young's modulus E_1 and Poisson's ratio μ_{12}

A longitudinal force is applied in the direction x; a stress σ_1 is generated. Apparent structural properties similar to the previous sub-section can be calculated. Axial and transverse displacement under external stress σ_1 is determined as follows:

$$\delta_{AL} = \frac{PL^2 \cos\theta K_{55}}{L^2 K_{44} K_{55} - 12(K_{46})^2} \tag{17}$$

$$\delta_{TL} = \frac{P\left(L^2 \sin\theta K_{55} K_{44} + 6L\cos\theta K_{55} K_{46} - 12\sin\theta \left(K_{46}\right)^2\right)}{K_{55}\left(K_{44}K_{55}L^2 - 12(K_{46})^2\right)} \tag{18}$$

Axial and transverse displacement under the influence of an external magnetic field is determined as follows:

$$\delta_{AM} = \frac{F_m L^2 K_{55} - 12 M_m K_{46}}{L^2 K_{44} K_{55} - 12(K_{46})^2} \tag{19}$$

$$\delta_{TM} = 6L\left(\frac{F_m K_{46} - M_m K_{44}}{L^2 K_{44} K_{55} - 12(K_{46})^2}\right) \tag{20}$$

Total axial and transverse displacement due to mechanical force and magnetic force are,

$$\delta_{TA} = \delta_{AL} + \delta_{AM}; \quad \delta_{TT} = \delta_{TL} + \delta_{TM} \tag{21}$$

Total displacement in direction 1 and direction 2 for single slant beam are, respectively:

$$\begin{aligned} \delta_1 &= \delta_{TA}\cos\theta + \delta_{TT}\sin\theta \\ \delta_2 &= -\delta_{TA}\sin\theta + \delta_{TT}\cos\theta \end{aligned} \tag{22}$$

Strain in direction 1 and direction 2 are respectively,

$$\varepsilon_1 = \frac{2\delta_1}{2L\cos\theta}; \quad \varepsilon_2 = -\frac{2\delta_2}{2L(\beta + \sin\theta)} \tag{23}$$

Apparent Young's modulus and Poisson's ratio of a unit cell in direction 1 are,

$$E_1 = \frac{\sigma_1}{\varepsilon_1}; \quad \mu_{12} = -\frac{\varepsilon_2}{\varepsilon_1} \tag{24}$$

2.2.2 Transverse Young's modulus E_2 and Poisson's ratio μ_{21}

When an extensional force W is applied in the direction y at the ends of the unit cell, as shown in Fig. 1a, a stress σ_2 is generated. Based on this force, apparent structural properties are calculated. The force is given as

$$W = 2\sigma_2 L W_{Rs}\cos\theta \tag{25}$$

Axial and transverse displacement of slant beams and axial displacement of vertical beam under external stress σ_2 is determined as follows:

$$\delta_{AL} = \frac{W L^2 \sin\theta K_{55}}{L^2 K_{44} K_{55} - 12(K_{46})^2} \tag{26}$$

$$\delta_{TL} = \frac{W\left(L^2\cos\theta K_{55} K_{44} + 6L\sin\theta K_{55} K_{46} - 12\cos\theta \left(K_{46}\right)^2\right)}{K_{55}\left(K_{44}K_{55}L^2 - 12(K_{46})^2\right)} \tag{27}$$

$$\delta_{AV} = \frac{2W}{K_{44}} \tag{28}$$

Axial and transverse displacement under an external magnetic field is determined as follows:

$$\delta_{AM} = \frac{F_m L^2 K_{55} - 12 M_m K_{46}}{L^2 K_{44} K_{55} - 12 (K_{46})^2} \tag{29}$$

$$\delta_{TM} = 6L \left(\frac{M_m K_{44} - F_m K_{46}}{L^2 K_{44} K_{55} - 12 (K_{46}^2)} \right) \tag{30}$$

Total axial and transverse displacement due to mechanical force and magnetic force,

$$\delta_{TA} = \delta_{AL} + \delta_{AM}; \quad \delta_{TT} = \delta_{TL} + \delta_{TM} \tag{31}$$

Total displacement in direction 1 and direction 2 for single slant beam are, respectively,

$$\begin{aligned} \delta_1 &= \delta_{TA} \cos\theta - \delta_{TT} \sin\theta \\ \delta_2 &= \delta_{TA} \sin\theta + \delta_{TT} \cos\theta + \delta_{AV} \end{aligned} \tag{32}$$

Strain in direction 2 and direction 1 are, respectively,

$$\varepsilon_2 = \frac{2\delta_2}{2L(\beta + \sin\theta)}; \quad \varepsilon_1 = -\frac{2\delta_1}{2L\cos\theta} \tag{33}$$

Apparent Young's modulus and Poisson's ratio of a unit cell in direction 2 are,

$$E_2 = \frac{\sigma_2}{\varepsilon_2}; \quad \mu_{21} = -\frac{\varepsilon_1}{\varepsilon_2} \tag{34}$$

3 CROSS SECTIONAL VARIATION

A comparative study on the apparent elastic properties has been carried out by varying the cross-sectional shapes of beams of the hybrid honeycomb structure. This modified structure will enable better control over the structural property. Two shapes, i.e., I-section and T-section, are considered along with the rectangular section.

3.1 Formulation for I-section

The cross-section of a beam of the lattice is considered to be an I-section. Longitudinal forces are provided in a similar direction to those discussed in the previous section. The apparent structural properties of such a structure are now calculated. Additional non-dimensional terms considered here are:

$$\alpha_I = \frac{T_m}{T_{Is}}; \quad \zeta_I = \frac{T_{Is2}}{T_{Is1}}; \quad \psi_I = \frac{W_{Is2}}{W_{Is1}}; \tag{35}$$

Substrate's neutral axis is located at $y_{Isn} = \frac{T_{Is}}{2}$

$$\begin{aligned} \int_s y dA &= -(h_{I1} - y_{Isn}) (2 W_{Is1} T_{Is1} + W_{Is2} T_{Is2}) \\ \int_m y dA &= \left[\left(T_{Is} + \frac{T_m}{2} \right) - h_{I1} \right] (T_m W_m) \end{aligned} \tag{36}$$

$$Y_s \int_s ydA + Y_m \int_m ydA = 0 \tag{37}$$

Solving Eqn. 37 using Eqn. 36,

$$h_{I1} = \frac{T_{Is}\left[1 + \frac{\psi_I \zeta_I}{2} + k_t \alpha_I (2+\zeta_I)\left(1+\frac{\alpha_I}{2}\right)\right]}{(2+\psi_I\zeta_I) + k_t\alpha_I(2+\zeta_I)} \tag{38}$$

Similarly,

$$\begin{aligned} &h_{I2} = h_{I1} - \frac{T_{Is}}{2+\zeta_I}; \quad h_{I3} = T_{Is}\left(1 - \frac{1}{2+\zeta_I}\right) - h_{I1}; \\ &h_{I4} = T_{Is} - h_{I1}; \quad h_{I5} = T_{Is}(1+\alpha_I) - h_{I1} \end{aligned} \tag{39}$$

Using the dimensions as Eqn. 39, the apparent Young's modulus and Poisson's ratio of the structure is calculated using similar formulation as developed in Section 2.1 and Section 2.2.

3.2 Formulation for T-section

In further analysis, the beam's cross-section is varied to T-section to determine the implication on apparent structural properties of the lattice metamaterial. Similar to the last discussion, additional non-dimensional terms assumed here are:

$$\alpha_T = \frac{T_m}{T_{Ts}}; \quad \zeta_T = \frac{T_{Ts2}}{T_{Ts1}}; \quad \psi_T = \frac{W_{Ts2}}{W_{Ts1}}; \tag{40}$$

$$\begin{aligned} y_{Tsn} &= \frac{(W_{Ts1}T_{Ts1})\left(T_{Ts2} + \frac{T_{Ts1}}{2}\right) + (W_{Ts1}T_{Ts1})\left(\frac{T_{Ts2}}{2}\right)}{(W_{Ts1}T_{Ts1}) + (W_{Ts2}T_{Ts2})} \\ &= \frac{T_{Ts1}\left[\left(\zeta_T + \frac{1}{2}\right) + \left(\psi_T \frac{\zeta_T^2}{2}\right)\right]}{1+\psi_T\zeta_T} \end{aligned} \tag{41}$$

$$\begin{aligned} \int_s ydA &= -\left(h_{T1} - y_{Tsn}\right)\left(W_{Ts1}T_{Ts1} + W_{Ts2}T_{Ts2}\right) \\ \int_m ydA &= \left(T_{Ts} + \frac{T_m}{2} - h_{T1}\right)\left(W_m T_m\right) \end{aligned} \tag{42}$$

$$Y_s \int_s ydA + Y_m \int_m ydA = 0 \tag{43}$$

Solving Eqn. 42 using Eqn. 43,

$$h_{T1} = \frac{T_{Ts}\left[k_t\alpha_T\left(1+\frac{\alpha_T}{2}\right) + \left(\frac{1+2\zeta_T+2\psi_T\zeta_T^2}{2(1+\zeta_T)^2}\right)\right]}{\left(\frac{1+\psi_T\zeta_T}{1+\zeta_T} + k_t\alpha_T\right)} \tag{44}$$

Similarly, dimensions with respect to the neutral axis are,

$$h_{T2} = T_{Ts}(1+\alpha_T) - h_{T1}; \quad h_{T3} = T_{Ts}\left(\frac{\zeta_T}{1+\zeta_T}\right) - h_{T1}; \quad h_{T4} = T_{Ts} - h_{T1} \tag{45}$$

The dimensions of Eqn. 45 are used with the formulation of Section 2.1 and Section 2.2 to determine the apparent structural properties.

4 RESULTS AND DISCUSSION

Existing literature by Gibson et.al. suggests that altering the cell angle in a honeycomb lattice structure should result in variation in the magnitude of the structural properties, like Young's modulus, without any indication of the sign reversal. An investigation has been conducted, considering PLA as the substrate and Terfenol-D as the smart material. The properties of materials and dimensions are listed in Table 1. Results based on the tabulated parameters and the formulation of the hybrid structure of Singh et.al. were plotted as Fig. 3a for the conditions with complete absence of magnetic field. However, a distinct sign reversal was observed for some thickness ratio conditions. As the thickness ratio increases, it is observed that the irregularity becomes more prominent.

Parameters	**Magnitude**
Young's modulus of PLA (Y_s)	$3.5GPa$
Young's modulus of Terfenol-D (Y_m)	$25GPa$
Magnetostrictive constant (d)	$3.7 \times 10^{-9} mA^{-1}$
Thickness of substrate (T_s)	$2mm$
Width of substrate (W_s)	$100mm$
Length of substrate (L)	$10mm$
Vertical substrate length (h)	$25mm$

Table 1: Material properties and dimensions of the hybrid lattice

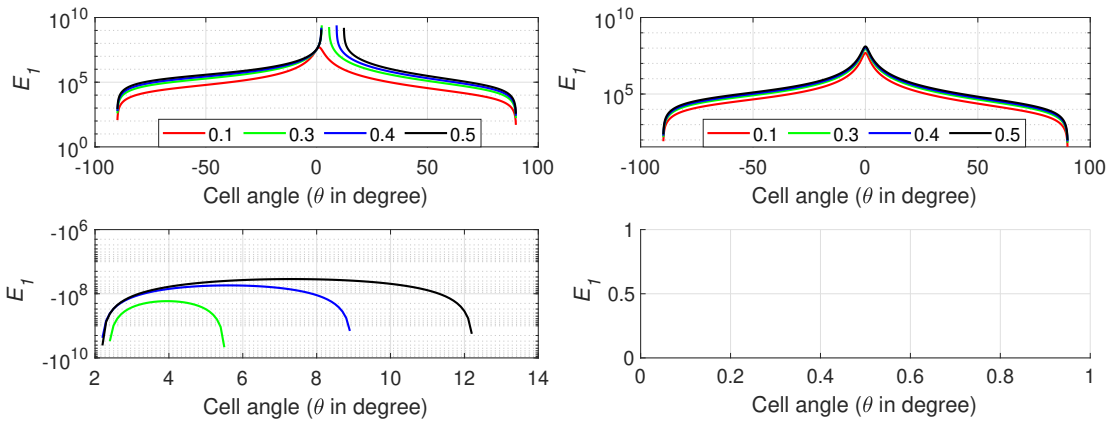

(a) **(b)**

Figure 3: Young's modulus plot for the condition in the absence of magnetic field **(a)** based on literature **(b)** after modification

Further investigation indicates that there is an assumption regarding the location of the neutral

axis, which is valid only when the thickness of the smart material is less compared to the substrate materials. The neutral axis represents the axis of the beam with zero stress. However, earlier literature [17] assumed that the neutral axis is present simply on the geometric centre of the substrate beam; this assumption only works well with a low-thickness smart layer. However, as the thickness ratio increases, the irregularities are seen in the result of the apparent structural properties.

The current paper proposes that the neutral axis will not always remain at the geometrical midline. Instead it will depend on the material properties of the structure as well as the thickness of the individual layers. Section 2 includes this idea, and the apparent Young's modulus result is plotted in Fig. 3b. The result now justifies the findings of Gibson et.al. with no sign reversal for the condition without applying a magnetic field. As the thickness ratio varies, a similar trend is observed. Results according to literature and after modification are plotted in Fig. 3.
The apparent structural properties of the I-section and T-section are plotted, as determined in Section 3.1 and Section 3.2. The properties strongly correlate with the cell angle, as seen in the equations; thus, with the change in angle, there is a gradual change in the magnitude of the structural parameters. A $2mm$ magnetostrictive sheet layer is used as the smart layer with the lattice structure. Thus, there will be a deformation in the structure in the presence of the magnetic field.

Variation in longitudinal Young's modulus (E_1), transverse Young's modulus (E_2), and Poisson's ratios (μ_{12} and μ_{21}) under the influence of externally applied forces has been depicted in Fig. 4. Here, the cross-sectional area of all three shapes is taken to be the same to get a fair comparison and to understand the variation in the elastic properties when only the first and second moment of the area varies. Dimension of the cross-sectional shapes has been taken in such a way that the T-section shows the highest first and second moments of area, the I section shows the intermediate, and the rectangular section shows the least. The Young's modulus of the structure depends on the ratio of the applied mechanical force to the induced strain. The strain comes out to be a function of the first and second moment of area, the variation in strain is affected significantly with the change in the first and second moment of area. A plot indicating the variation of E_1 and E_2 has been plotted in Fig. 4a and 4b, in both the figures, it can be observed that for all the cell angles, the highest/ lowest value of E_1 and E_2 is for the shape which has the highest/ lowest first and second moment of area, which is exhibited by T shape and rectangular shapes respectively. However, there is no significant difference in Poisson's ratio plots. Poisson's ratio is the ratio between strains in x and y directions, respectively. Here, the strain terms mutually cancel out the effect of the moment of areas; thus, there is a subtle difference in the magnitude while varying the cross-sectional shape.

Further, when the magnetic field is applied to the lattice structure along with externally applied force, the properties of the structure have been obtained and plotted in Fig. 5. The ratio of magnetic field intensity to mechanical stress has been kept constant at a magnitude of 2000 to reduce the number of variables. Mechanical strain develops in the lattice due to the application of force. Moreover, an additional magnetostriction develops due to the application of the magnetic field. Depending upon the direction of the magnetic field and the magnetostrictive coefficient,

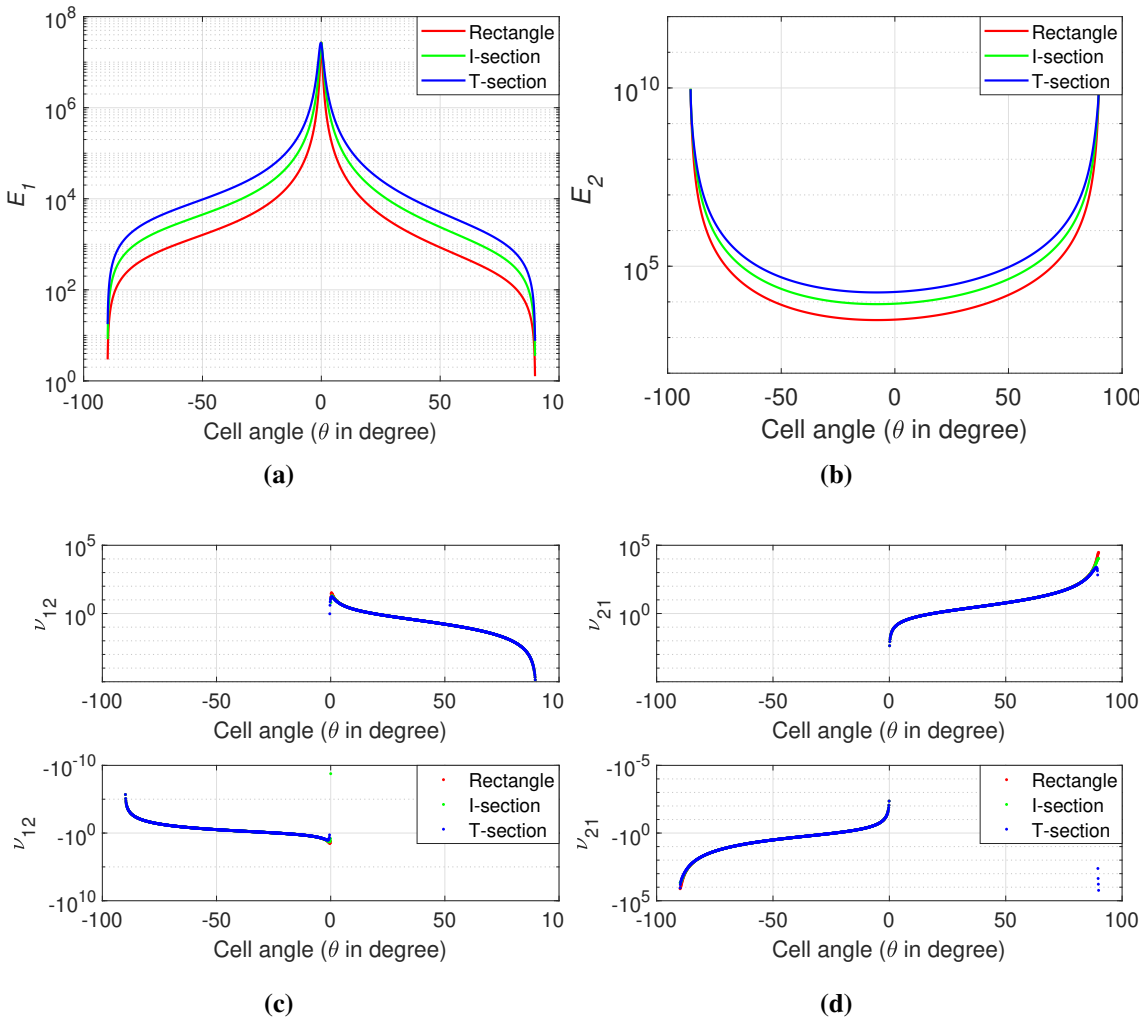

Figure 4: Comparison of mechanical properties between rectangular cross-section, I-section, and T-section with same total area of section at no magnetic field applied condition: (a) E_1 (b) E_2 (c) ν_{12} (d) ν_{21}

the overall strain either increases or decreases. Results have been plotted in Fig. 5, highlighting the T-section with the highest magnitude for E_1 and E_2 and the rectangular section with the lowest. It is noted that the magnitude of Young's modulus follows a similar trend, justifying our conclusion on the dependence of the first and second moment of inertia. Further, at some cell angles the reversal of the elastic properties can be observed. This unique behaviour exists when the magnetostrictive strain is higher than the mechanical strain, and it acts in opposite directions to each other. The plots in Fig. 5a and 5b depict that the sign reversal occurs in all three cases. However, the sign reversal takes place at different cell angles for the different cases. In Fig. 5c and 5d, it can be observed that for Poisson's ratio, the sign reversal is only observed for the

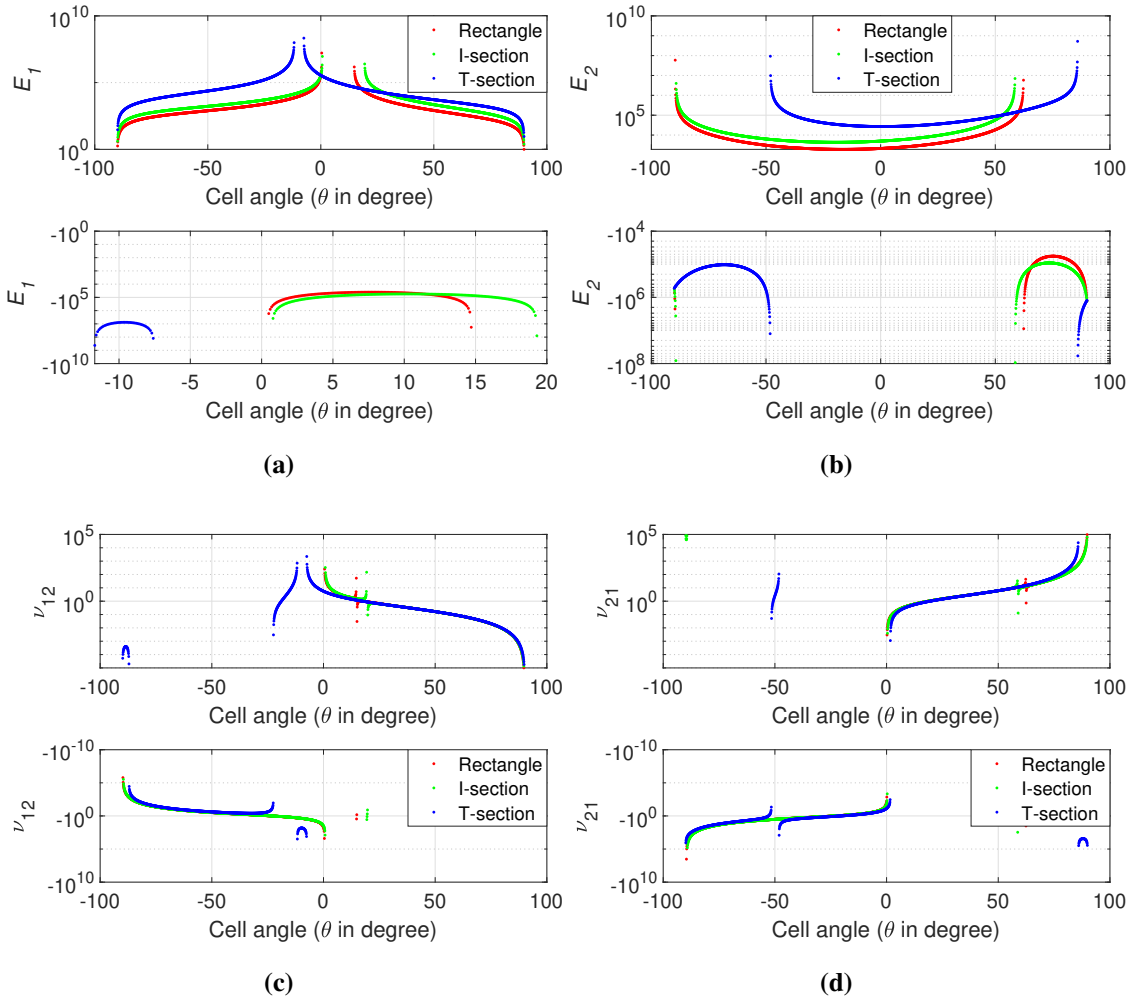

Figure 5: Comparison of mechanical properties between rectangular cross-section, I-section, and T-section with same total area of section and magnetic field to stress ratio of 2000: (a) E_1 (b) E_2 (c) ν_{12} (d) ν_{21}

rectangular and I section cross-section, but in the T section, no sign reversal is there. This is due to the high first and second moment of area for the T section, which offers high resistance to induced strains.

5 CONCLUSION

This paper proposes an improved procedure for obtaining apparent structural properties of hybrid lattice metamaterial. Some assumptions considered in the previous work limited the potential of such hybrid structures for their application in developing futuristic materials. The neutral axis was considered to be positioned exactly at the geometric mid-line of a cross-section. Although

this assumption works well for hybrid structures when a thin layer of smart material is used, however, irregularities are observed at a higher thickness ratio of the smart layer. Thus, accurate determination of the neutral axis is necessary to obtain reliable apparent structural properties. Necessary calculation is carried out to obtain the modified position of the neutral axis.
In addition, a study on the effect of variation of cross-section shapes of beams in a lattice structure is done to study the fluctuation of the magnitude of the properties with cross-section and cell angle. A strong dependence of the first and second moments of the area is found in Young's modulus of the hybrid structure. The rectangular section shows the lowest apparent Young's modulus, followed by the I-section and the T-section with the highest, which is also the order of their first and second moment of area. However, Poisson's ratio is independent of variation in the cross-sectional shapes, as it is the ratio of strains, and the effect of the variation in the cross-sectional shape gets cancelled out every time. Finally, a distinct sign reversal is observed in E_1, E_2, ν_{12} and ν_{21} due to the combined effect of mechanical strain and magnetostriction. The range of cell angle for this unique phenomenon shifts with the variations in the cross-section of a beam of the lattice structure.

REFERENCES

[1] Greaves, George Neville, A. Lindsay Greer, Roderic S. Lakes, and Tanguy Rouxel. "Poisson's ratio and modern materials." Nature materials 10, no. 11 (2011): 823-837.

[2] Mukherjee, Sushovan, Fabrizio Scarpa, and S. Gopalakrishnan. "Phononic band gap design in honeycomb lattice with combinations of auxetic and conventional core." Smart Materials and Structures 25, no. 5 (2016): 054011.

[3] Dwivedi, Ankur, Arnab Banerjee, and Bishakh Bhattacharya. "Dynamics of piezo-embedded negative stiffness mechanical metamaterials: A study on electromechanical bandgaps." In ASME International Mechanical Engineering Congress and Exposition, vol. 84478, p. V001T01A015. American Society of Mechanical Engineers, 2020.

[4] Vallecchi, A., F. Capolino, and A. G. Schuchinsky. "2-D isotropic effective negative refractive index metamaterial in planar technology." IEEE microwave and wireless components letters 19, no. 5 (2009): 269-271.

[5] Bertoldi, Katia, Pedro M. Reis, Stephen Willshaw, and Tom Mullin. "Negative Poisson's ratio behavior induced by an elastic instability." Advanced materials (2010).

[6] Gatt, Ruben, and Joseph N. Grima. "Negative compressibility." physica status solidi (RRL)–Rapid Research Letters 2, no. 5 (2008): 236-238.

[7] Christensen, Johan, Muamer Kadic, Oliver Kraft, and Martin Wegener. "Vibrant times for mechanical metamaterials." Mrs Communications 5, no. 3 (2015): 453-462.

[8] Zenkert, Dan. "An introduction to sandwich structures." (1995).

[9] Ashby, Michael F., and Lorna J. Gibson. "Cellular solids: structure and properties." Press Syndicate of the University of Cambridge, Cambridge, UK (1997): 175-231.

[10] Ajdari, Amin, Babak Haghpanah Jahromi, Jim Papadopoulos, Hamid Nayeb-Hashemi, and Ashkan Vaziri. "Hierarchical honeycombs with tailorable properties." International Journal of Solids and Structures 49, no. 11-12 (2012): 1413-1419.

[11] Mukhopadhyay, Tanmoy, Jiayao Ma, Huijuan Feng, Degao Hou, Joseph M. Gattas, Yan Chen, and Zhong You. "Programmable stiffness and shape modulation in origami materials: Emergence of a distant actuation feature." Applied Materials Today 19 (2020): 100537.

[12] Adhikari, Sondipon, T. Mukhopadhyay, Alexander Shaw, and N. P. Lavery. "Apparent negative values of Young's moduli of lattice materials under dynamic conditions." International Journal of Engineering Science 150 (2020): 103231.

[13] Singh, A., T. Mukhopadhyay, S. Adhikari, and B. Bhattacharya. "Active multi-physical modulation of Poisson's ratios in composite piezoelectric lattices: on-demand sign reversal." Composite Structures 280 (2022): 114857.

[14] Grima, Joseph N., Roberto Caruana-Gauci, Mirosław R. Dudek, Krzysztof W. Wojciechowski, and Ruben Gatt. "Smart metamaterials with tunable auxetic and other properties." Smart Materials and Structures 22, no. 8 (2013): 084016.

[15] Dwivedi, Ankur, Arnab Banerjee, and Bishakh Bhattacharya. "A novel approach for maximization of attenuation bandwidth of the piezo-embedded negative stiffness metamaterial." In Active and passive smart structures and integrated systems XIV, vol. 11376, pp. 478-485. SPIE, 2020.

[16] Singh, A., T. Mukhopadhyay, Sondipon Adhikari, and B. Bhattacharya. "Voltage-dependent modulation of elastic moduli in lattice metamaterials: Emergence of a programmable state-transition capability." International Journal of Solids and Structures 208 (2021): 31-48.

[17] Singh, A., T. Mukhopadhyay, S. Adhikari, and B. Bhattacharya. "Extreme on-demand contactless modulation of elastic properties in magnetostrictive lattices." Smart Materials and Structures 31, no. 12 (2022): 125005.